Stall Buffet Modeling using Swept Wing Flight Test Data

Marschalk, S.; Luteijn, P.C.; van Os, D.; Pool, D.M.; de Visser, C.C.

DOI
10.2514/6.2021-0286

Publication date
2021

Document Version
Final published version

Published in
AIAA Scitech 2021 Forum

AIAA SciTech Forum
11–15 & 19–21 January 2021, VIRTUAL EVENT
AIAA Scitech 2021 Forum

10.2514/6.2021-0286

Stall Buffet Modeling using Swept Wing Flight Test Data

Sven Marschalk* and Peter C. Luteijn†
Delft University of Technology, Delft, The Netherlands

Dirk van Os‡
Fokker Services | A GKN Aerospace Company, Hoofddorp, The Netherlands

Daan M. Pool§ and Coen C. de Visser¶
Delft University of Technology, Delft, The Netherlands

As of April 2019, upset prevention and recovery training in flight simulation training devices is a mandatory practice for commercial and civil aircraft pilots. Aircraft stalls are a well-known upset type, therefore simulation of aircraft stall behavior is required. A key characteristic of stalls is the stall buffet, which in current stall models is still insufficiently modeled. In this research, a new methodology to more accurately model stall buffet behavior derived from swept wing flight test data is presented. Buffet effects occur after exceeding the critical angle of attack, with an aircraft type-specific buffet onset duration to fully develop the maximum buffet intensity. The buffet transient behavior is modeled with a frequency response fit and a multivariate second-order polynomial to capture aircraft eigenmode-shape frequencies and state dependent buffet intensity, respectively. Aircraft recovery and thus receding buffet effects occur as the angle of attack starts increasing again after the initial recovery dip, which is used as buffet offset scheduling parameter. Generalization of the results was shown with the validation of data set of a straight-wing aircraft, which indicates a step towards a more generic stall buffet model methodology.

Nomenclature

A_Y, A_Z	Specific forces along body axis in Y and Z direction [m/s^2]	Q	Quality factor [-]
A	Aspect ratio [-]	X	Flow separation point [-]
b	Wing span [m]	*Greek*	
C_L	Lift coefficient [-]	α	Angle of attack [rad]
c	Mean aerodynamic chord [m]	$\dot{\alpha}$	Rate of change in angle of attack [rad/s]
f	Frequency [Hz]	γ	Standard deviation
f_s	Sample frequency [Hz]	Λ	Wing sweep angle at c/4 [-]
H	Transfer Function	$\hat{\zeta}$	Parameter estimates
K	Gain [-]	σ	Parameter standard deviation
k_{shift}	Shifting factor	σ^2	Parameter variance
m	Mass [kg]	ω	Frequency [rad/s]
N	Number of peaks		
S	Wing surface area [m^2]		
V_{TAS}	True airspeed [m/s]		

I. Introduction

The buffet is the aerodynamic excitation due to flow separation causing pressure fluctuations over the wing, which induces aircraft structural vibrations known as buffeting [1, 2]. Buffeting occurs at high angles of attack or high Mach numbers and negatively affects aircraft aerodynamic performance. In-flight buffeting degrades aircraft handling qualities and causes structural damage, which could induce structural fatigue if sustained over an extended period of time [3]. Therefore, aircraft manufactures determine buffet characteristics and envelopes in the early design stage [4, 5].

*MSc student, Control & Simulation Section, Faculty of Aerospace Engineering, Kluyverweg 1, 2629HS, Delft, The Netherlands.
†MSc student, Control & Simulation Section, Faculty of Aerospace Engineering, 2629HS, Delft, The Netherlands.
‡Chief Engineer, Fokker Services | A GKN Aerospace Company, Hoeksteen 40, 2132 MS Hoofddorp, The Netherlands.
§Assistant Professor, Control & Simulation Section, Faculty of Aerospace Engineering, P.O. Box 5058, 2600GB Delft, The Netherlands; d.m.pool@tudelft.nl. Senior Member AIAA.
¶Assistant Professor, Control & Simulation Section, Faculty of Aerospace Engineering, P.O. Box 5058, 2600GB Delft, The Netherlands; c.c.devisser@tudelft.nl. Member AIAA.

In early studies on aircraft buffet, 2D wing models were used in wind-tunnel experiments to determine buffet effects at a certain combination of Mach number, Reynolds number and angle of attack [6–8]. These 2D wing models used strain gauges to measure the wing root bending moments, where compliance was shown by correlation of results to flight test data. Research into the transonic flight envelope led to the prediction of buffet onset and maximum buffet load using pressure measurements [1]. A combination of Computational Fluid Dynamics (CFD) calculations and wind-tunnel tests led to increased accuracy of buffet characteristics, such as buffet intensity and buffet onset [4, 9]. In an experimental wind-tunnel setup multiple buffet onset prediction indicators were defined and compared with each other [10]. These buffet onset indicators are the Root Mean Square (RMS) signal variations of root strain gauges, RMS signal variations of wingtip accelerations measured with accelerometers, lift curve slope reduction, pitch moment break, axial force break and trailing edge pressure divergence [3]. The pitching moment break and lift curve slope break method proved to be inadequate to determine buffet onset when validated using flight test data [3, 11]. Additionally, a buffet intensity parameter was defined using strain gauge responses and wind tunnel ambient unsteadiness, to determine the influence of aircraft characteristics on buffeting behavior [12]. A less commonly used parameter defined buffet intensity using the total damping, wingtip accelerations, and generalized mass [13]. Buffet intensity was categorized in light, medium and heavy buffeting. In a more recent study, fractional change transformations to determine the buffet flight envelope for a generic transport aircraft in the conceptual design stage using the aircraft wing geometries as input [14]. Although proven adequate, the approach required a generic reference buffet onset curve or a seed aircraft with a known buffet onset curve.

A leading cause of aircraft accidents and incidents in commercial and civil aviation over the last decade is Loss of Control-Inflight (LOC-I) [15–17]. Therefore, mitigation of LOC-I occurrences has become a priority. Near-term mitigation solutions focus on aircraft loss of control prevention as well as aircraft recovery training, commonly referred to as Upset Prevention and Recovery Training (UPRT) [18–20]. Well-known and recurrent types of upset conditions which lead to LOC-I are aircraft stalls [21, 22]. As of April 2019, regulatory frameworks make UPRT mandatory for aircraft pilots for pilot training in Flight Simulation Training Devices (FSTD) [21, 23]. UPRT requires accurate stall models, to simulate aircraft stall behavior in FSTD.

A key characteristic of a stall is the buffet, as buffeting is an initial cue for pilots which indicates entering of the unsafe part of the flight envelope. The European SUPRA project produced enhanced aerodynamic models, based on a combination of wind-tunnel data and CFD results, for simulator environments including cueing solutions providing better and realistic buffet feedback [24]. Buffet frequency was modeled according to three structural modes and intensity was gradually increased with the angle of attack. Buffet onset was defined as exceeding the critical angle of attack, varying with Mach number. An approach to model buffet using flight test data has been used in [25] which is based on Kirchoff's theory on flow separation. Buffet onset is modeled by exceeding a fixed flow separation-parameter (X) threshold, whereas the frequency was identified using power spectral density analysis of the acceleration measurements. Lastly, the intensity was modeled using the X-parameter and a fixed gain. A common deficiency, which remains in current aircraft stall models is the insufficient haptic and physical vibratory feedback of buffeting felt by pilots in stalled conditions when flying in an FSTD [26, 27].

The main contribution of this paper is a new methodology for modeling the stall buffet component using swept wing flight test data from a medium-sized transport aircraft, namely the Fokker-100. A robust and generalized methodology was proven when validated using flight test data of a straight wing business jet aircraft, namely the Cessna Citation II. However, the generalization of the methodology is dependent on the availability of type-specific aircraft parameters identified from the flight test data. In the upcoming section, an introduction on the flight test data acquisition vehicle is presented. Secondly, the third section covers the stall buffet modeling methodology. Thereafter, the results of the methodology are discussed and lastly, the final section concludes the presented research.

II. Flight Test Data Acquisition Vehicle

The flight test data acquisition vehicle in this research is the Fokker-100 aircraft. The Fokker-100 is a regional jet with twin rear fuselage-mounted engines and a T-tail configuration used for short to medium range type of operations. Figure 1 depicts a schematic overview of the Fokker-100, which also includes the defined body-axis reference system.

The aircraft was equipped with a flight test instrumentation system that logged the sensor measurements in a Flight Test Data Processing System (FDVS) database. A subsystem of the flight test instrumentation system used these sensor measurements to perform real-time calculations. An overview of relevant flight test instrumentation systems in this research is presented next.

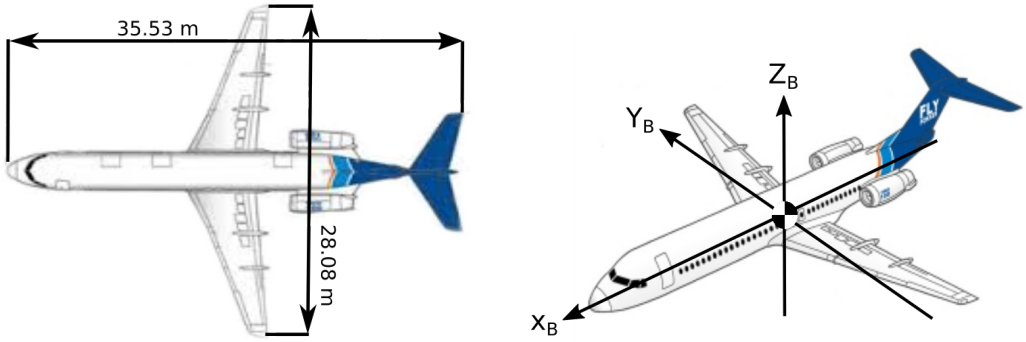

Fig. 1 A schematic overview of the Fokker-100 dimensions and the body reference frame axes definition.

A. Flight Test Instrumentation

In this research two flight data instrumentation subsystems which provide sensor measurements are used. The two flight data instrumentation subsystems are the Air Data System (ADS) and the Inertial Reference System (IRS). Additionally, an in-flight mass measurement was provided by the Flight Management System (FMS).

The ADS system consists of four subsystems, which are the pitot-static systems, angle of attack vanes, temperature probes and the Air Data Computers (ADC). The IRS entails three subsystems, which are two Inertial Reference Systems, Mode Select Unit (MSU) and an Inertial System Display Unit (ISDU). Static and pitot pressure is supplied to various instruments and systems including the ADC by three independent pitot-static systems, which consist of three pitot tubes and three static ports. Both angle of attack vanes provide the angle of attack information to the stall prevention systems, i.e., the ADC and the Automatic Flight Control and Augmentation System (AFCAS). Each ADC converts input signals from the angle of attack sensors, pitot-static system, outside air temperature probes and Altimeter Set Panel (ASP) into electrical signals, which are supplied to other various systems such as the AFCAS and IRS. Attitude and navigation information is supplied by the IRS. The IRS measures body-specific forces and body axis rotational rates, which are combined with the V_{TAS} measurements of the ADC to increase airspeed accuracy. The IRS instrumentation system was located close to the center of gravity. IRS output signals provide information to various flight and navigation systems, including the Flight Management System (FMS). All relevant measured parameters and the respective update frequencies and measures of accuracy can be found in Table 1.

Table 1 Parameters measured by ADS and AHS.

Symbol	f_s	σ^2	Source
α	16 Hz	$2.81 \cdot 10^{-6}$ rad	Left α vane
α	16 Hz	$2.32 \cdot 10^{-6}$ rad	Right α vane
A_Y	50 Hz	$8.27 \cdot 10^{-4}$ m/s^2	IRS
A_Z	50 Hz	$4.10 \cdot 10^{-3}$ m/s^2	IRS
V_{TAS}	8 Hz	$8.76 \cdot 10^{-2}$ m/s	ADC 1
V_{TAS}	8 Hz	$9.13 \cdot 10^{-2}$ m/s	ADC 2
m	40 Hz	$9.60 \cdot 10^{2}$ kg	FMS 1
m	40 Hz	$9.60 \cdot 10^{2}$ kg	FMS 2

B. Flight Test Maneuvers

As part of regulatory compliance Fokker conducted certification flight tests to acquire stall certification data. Stall maneuvers were conducted according to JAR 25.201 and JAR 25.203. JAR stall maneuvers have to be conducted in both straight flight and 30 degrees banked turns, with power off and with the power necessary to maintain 1.6 V_S, where V_S is the stall speed with flaps in approach configuration, gear retracted and maximum landing weight. Additionally, compliance is also shown in any aircraft configuration, i.e., all possible positions combinations of deceleration devices, flaps and landing gear, with representative weights within the certification range. In this research, only stall maneuvers in straight flight, i.e., wings-level, in clean and landing configuration are considered. A wings-level stall maneuver is initiated at an airspeed sufficiently above the stall speed, to ensure a steady deceleration rate of one knot per second until the aircraft is stalled or aircraft control reaches a stop. Normal recovery procedures are initiated by either the pilot or the stick pusher when acceptable stall behavior is noticeable or detected. Stall behavior is considered acceptable when the pilot has a clear and distinctive indication that the aircraft has entered a stall condition. Acceptable stall indications are a not immediately controllable nose-down pitching moment, which may be accompanied by a simultaneously not immediately controllable rolling motion, severe buffeting effects in terms of magnitude and severity that are strong

and effective deterrents to further speed reduction, or a not immediately controllable significant roll in or out turn for dynamic stalls.

Prior to the JAR certification flight tests, Fokker also conducted stall maneuvers resembling JAR stalls in straight and turning flights. These stall maneuvers are characterized as idling stalls. A similar approach to the JAR flights was conducted, where the power levers were set to idling and the aircraft was trimmed at an airspeed within 1.2 V_S to 1.4 V_S prior to the stall. Approximate zero control inputs prior to the stall were applied to the rudder and ailerons, whereas a longitudinal control input on the elevator, prior to the stall, was applied to ensure the constant speed reduction of approximately 1 kts/s. All stall maneuvers were also flown in any likely combination of aircraft configurations. Normal recovery procedures were initiated when stalled conditions were perceived by the pilots or detected by the stall identification system, i.e., a stick pusher.

A total of 190 flight recordings were used to model the buffet model in two different flight conditions, namely the clean and landing aircraft configuration. A distinction in clean and landing was made as buffet effects are dependent on flight conditions, maneuvers, and aeroelastic aircraft characteristics [28]. A clean aircraft configuration is defined as the landing gear in the 'UP' position with flaps zero. A landing configuration is defined as landing gear in the 'DOWN' position with flaps maximum. A total of 92 recordings were flown in clean configuration, the remaining 88 recordings were therefore flown in landing configuration. In Figure 2 the flight envelope in terms of angle of attack and Mach number and pressure altitude and true airspeed is shown for both aircraft configurations, where the black dots indicate the training recordings and the red dots the validation recordings.

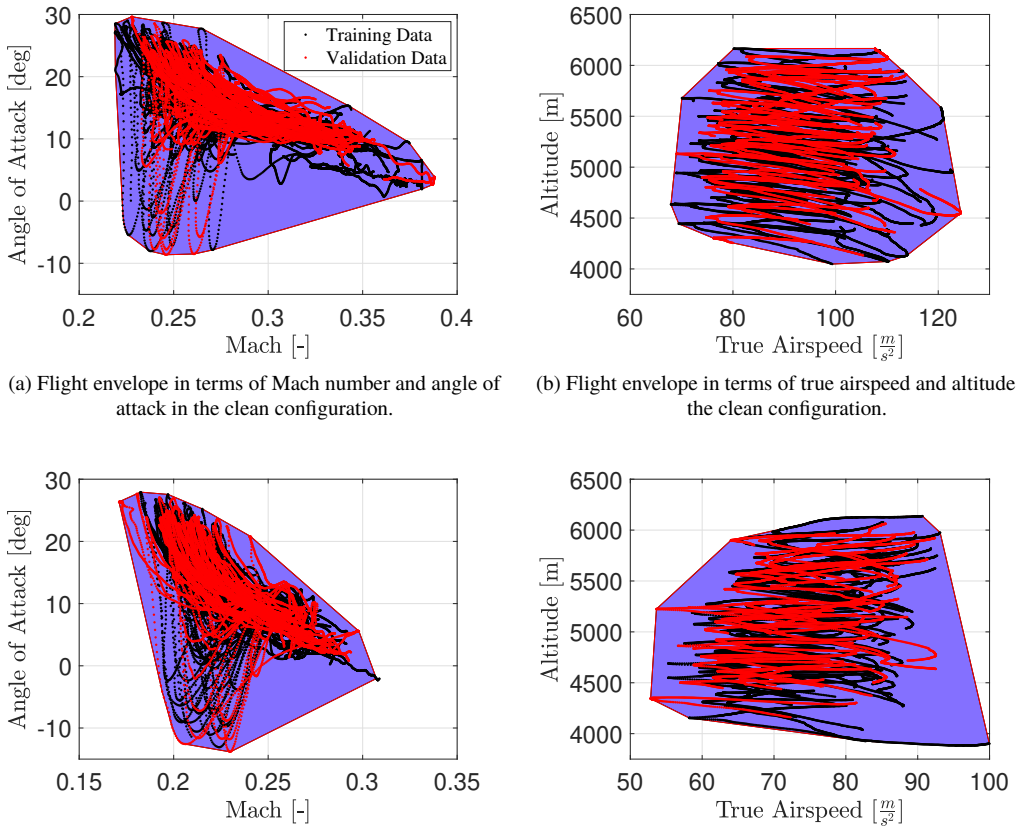

(a) Flight envelope in terms of Mach number and angle of attack in the clean configuration.

(b) Flight envelope in terms of true airspeed and altitude in the clean configuration.

(c) Flight envelope in terms of Mach number and angle of attack in the landing configuration.

(d) Flight envelope in terms of true airspeed and altitude in the landing configuration.

Fig. 2 Flight envelopes for the Fokker-100 in terms of Mach number, angle of attack, true airspeed, and altitude in the clean and landing configuration.

In the clean configuration, a valid buffet model is identified for angles of attack ranging from 10 degrees to 27 degrees, altitudes ranging from 4,200 meters to 6,100 meters, Mach numbers ranging from Mach 0.23 to Mach 0.37 or true airspeeds ranging from 70 m/s to 110 m/s. In the landing configuration the validity of the buffet model shifts

to angles of attack ranging from 5 degrees to 25 degrees, altitudes ranging from 4,000 meters to 6,200 meters, Mach numbers ranging from Mach 0.19 to Mach 0.28 or true airspeeds ranging from 60 m/s to 85 m/s. To model the buffet, a flight data recording separation of 60% and 40% was used, i.e., 60% of the data is used for model training purposes and 40% for model validation purposes.

C. Flight Test Data Pre- and Post-processing

An overview with relevant measured parameters for this research can be found in Table 1. A total of two additional, not readily available parameters are required, which are the lift coefficient C_L and the rate of change in the angle of attack $\dot{\alpha}$. Both parameters are, however, calculated in the subsystem of the flight test instrumentation. All measured parameters are filtered using a low-pass filter, which is a fourth-order Butterworth filter. The cut-off frequency is set at 1.5 Hertz, to remove the vibrations due to the stall buffet. A cut-off frequency of 1.5 Hertz is sufficient as buffet peak frequencies are higher than 2 Hertz, as can be seen in Figure 3. However, the cut-off frequency is a specific frequency for the Fokker-100 as buffet characteristics are aircraft dependent. A different cut-off frequency was used for filtering the Cessna Citation II data [25]. After filtering, a re-sampling procedure is required as sensor measurements had different sample frequencies and inconsistent recording lengths. All filtered parameters are re-sampled with a sampling frequency of 16 Hertz to comply with the calculations of Fokker. The re-sampled parameters α, V_{TAS} and m are averaged for each flight recording. A stall entry rate or deceleration rate is defined and calculated as the linear slope from the stall speed to an airspeed ten percent above the stall speed. Lastly, the filtered and re-sampled accelerations, in the vertical or the lateral directions, are defined as the baseline accelerations, which are part of the buffet model to simulate the vibrations of the buffet.

III. Methodology

The entire buffet model consists of four separate models, one for each combination of clean and landing configuration and lateral and vertical acceleration, which all use the same underlying methodology. First of all, the buffet onset and offset points, i.e., the activation and deactivation of the buffet model, are determined. Secondly, the transient buffet behavior is modeled, which determines the frequency and the intensity of the buffet. A frequency response fit in combination with a gain scheduling procedure using a multivariate polynomial form the basis of each separate buffet model. Lastly, the buffet models are added to the respective baseline accelerations in the respective configuration to represent the vibrations of the buffet.

A. Buffet On- and Offset Modeling

The buffet onset is defined as the point in time when high frequency oscillations appear in the measured accelerations. Correspondingly, the buffet offset is the point in time when these oscillations disapear behind the noise horizon. A modeling technique for buffet onset and offset conditions is exceeding a fixed parameter threshold. In the SUPRA model exceeding the critical angle of attack determines the onset and offset conditions for the buffet [24]. In [25] the buffet onset and offset conditions are modeled according to Kirchoff's X-parameter, where the buffet (de-)activation threshold was set at $X = 0.89$. However, modeling the buffet onset and offset using Kirchoff's X-parameter resulted in an unsatisfactory buffet (de)-activation for the Fokker-100, as the buffet onset and offset occurred at incorrect times, due to the fixed X-parameter.

In this research, the buffet onset is modeled based on exceeding the angle of attack at the maximum lift coefficient. Exceeding the angle of attack at maximum lift coefficient will change the slope in the $C_L - \alpha$ curve from positive to negative, thus the change in the sign is used as the activation for the buffet onset. To reduce the effects of measurement noise amplification due to differentiation towards α the slope of the $C_L - \alpha$ curve is computed using a weighted moving-average function in the form of:

$$(C_{L_\alpha})_j = \frac{1}{\mathbf{w}} \frac{\Delta C_{L_j}}{\Delta \alpha_j} \tag{1}$$

where C_{L_j} and α_j are the weighted average at point j and $\mathbf{w}$ is the sum of the weighting functions. C_{L_j} and α_j are calculated using Eq. (2):

$$\Delta P_j = \sum_{n=j-k_{shift}}^{n=j+k_{shift}} w_n \cdot [P(n) - P(n-1)] \quad \text{where} \quad P = \{C_L, \alpha\} \tag{2}$$

where k_{shift} determines the window size of the weighted function and w_n is the respective weighted value at point n. The window size and weighted values were set such that a clean signal was obtained for the Fokker-100 flight data. The window for the weighted average uses past and future data points, which makes it currently unusable for real-time applications. Removing future data points would make it suitable for real-time applications, however, would also decrease the smoothing accuracy. In addition to the smoothing function, an additional constraint is set, which is a minimum angle of attack at which buffet occurs. For the Fokker-100, the angle of attack for the buffet model to be activated has to exceed 17.5 degrees.

A similar approach is used to determine the buffet offset, i.e. when aircraft is recovered and buffeting ends. Buffet effects end when the angle of attack starts increasing again, hence the buffet offset is scheduled for increasing angles of attack during recovery. Depending on the severity and duration of the stall maneuver, the buffet offset varies with the angle of attack. Therefore, a positive rate of $\dot{\alpha}$ was found to suffice as the buffet offset. However, as flow attaches at lower angles of attack compared to flow separation an additional constraint was set. A change in sign of $\dot{\alpha}$ in combination with an angle of attack below 15 degrees is used as the buffet offset point. A first-order derivative of the angle of attack is calculated using a similar approach as for the buffet onset, namely a weighted moving average function.

B. Buffet Frequency and Transient Modeling

1. Buffet frequency response

A main characteristic of the buffet is captured in the frequency of the induced structural vibrations. The IRS in the Fokker-100 captures the structural vibrations by measuring the body accelerations, which are transformed into the frequency domain by applying a Fourier transform. A periodogram is obtained from the Fourier transform of the accelerations, which is the best possible estimate of a Power Spectral Density (PSD). An increase in accuracy is achieved by averaging multiple realizations for each periodogram. A periodogram for the accelerations measured at the IRS in the lateral and vertical direction for the clean configuration is shown in Figure 3.

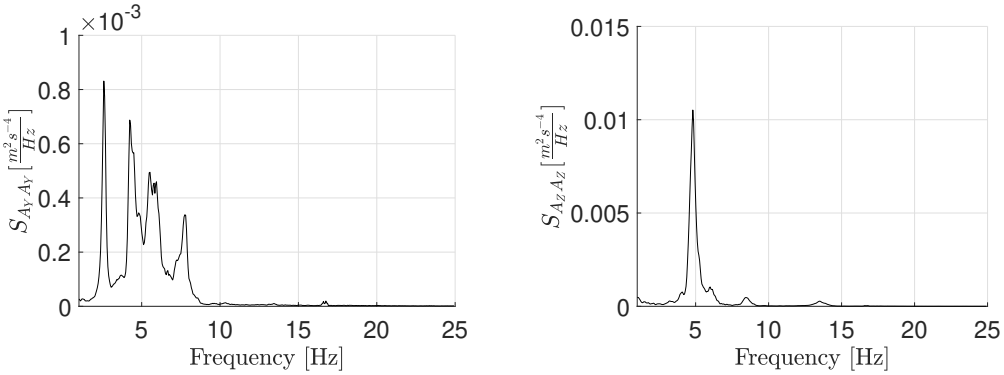

(a) Periodogram of the IRS acceleration measurements in lateral direction in the clean configuration.

(b) Periodogram of the IRS acceleration measurements in vertical direction in the clean configuration.

Fig. 3 Periodogram in lateral and vertical direction in clean configuration.

The periodogram in the longitudinal direction is omitted from this research as the intensity in the longitudinal direction is negligible. Figure 3 indicates a higher intensity in the vertical direction due to the order of magnitude difference, indicating that the buffet in the vertical direction is the strongest. A total of four peak frequencies in the lateral direction are identified, and a total of three peak frequencies in the vertical direction are identified. A buffet model frequency response fit is based on the identified peak frequencies in each direction, which is given by the following PSD relation:

$$S_{yy} = |H(j\omega)|^2 S_{uu}. \tag{3}$$

The shaping filter $H(j\omega)$ is used to model the buffet peak frequencies and a uniform white noise input signal u with an intensity equal to one is assumed. The shaping filter consists of a combination of several second-order band-pass filters:

$$H(j\omega) = \sum_{i=1}^{N} H_i(j\omega) = \sum_{i=1}^{N} \frac{K_i \frac{\omega_i}{Q_i} j\omega}{(j\omega_i)^2 + \frac{\omega_i}{Q_i} j\omega + \omega_i^2}, \tag{4}$$

where N is the number of band-pass filters equal to the number identified peak frequencies. A nonlinear least-squares method was used to estimate each shaping filter parameter. In `MATLAB` the function `nonlinsq` was used where the number of iterations, functions evaluations, and the Levenberg-Marquardt algorithm was set. An iterative outer loop calls the `nonlinsq` function to maximize the R^2 value, whereas the `nonlinsq` function minimizes the Mean Squared Error (MSE).

2. Buffet intensity scaling

Although buffet effects are present at buffet onset, the data showed that buffeting intensity scaled up gradually, to a certain maximum. This transient cannot be modeled with the frequency response function in Eq. (4). To obtain the transient, it is opted to include a quadratic polynomial scaling function (in time), which is supported by observing the transients in the flight data as well as findings from literature [28]. The quadratic scaling function is multiplied with the noise shaping filter after which we obtain a buffet onset model as follows:

$$A_{i,on}(t) = \frac{\hat{a}}{(t_e - t_s)^2}(t - t_s)^2 \mathcal{F}^{-1}(H(jw)u), \tag{5}$$

with t_s the buffet start time, t_e the buffet end time, $\mathcal{F}^{-1}$ the inverse Fourier transform, and with polynomial coefficient $\hat{a} = \frac{A_i}{2\sigma_i}$. A_i is defined as the maximum acceleration in the lateral ($i = Y$) or vertical ($i = Z$) direction and σ_i is defined as

$$\sigma_i = \sqrt{\frac{1}{N-1} \sum_{j=1}^{N} (A_i[j] - \mu_i)^2}, \tag{6}$$

with μ_i the average acceleration along the $i = Y$ or $i = Z$ axis. The buffet offset model, which is activated during stall recovery, is defined equivalently as:

$$A_{i,off}(t) = \frac{\hat{a}}{(t_e - t_s)^2}(t - t_e)^2 \mathcal{F}^{-1}(H(jw)u), \tag{7}$$

where in this case the quadratic scaling function vanishes to 0 as the buffet fades out. To simplify Eq. (5) and Eq. (7) and obtain a general model, an average buffet onset transient time is calculated for each buffet model, where the final buffet onset transient time is the median of all recordings.

C. Complete Fokker-100 Buffet Model

The combination of buffet onset and offset, buffet frequency and intensity are captured in the buffet model and the buffet is modeled according to Eq. (8):

$$A_{i,mod} = A_{i,filt} + B_i(x) \cdot A_{i,on/off} \tag{8}$$

where $A_{i,mod}$ is the model output in terms of the acceleration in lateral or vertical direction ($i = Y, Z$), $A_{i,filt}$ is the baseline acceleration in either direction, $B_i(x)$ is the flight-condition dependent buffet scaling and with $A_{i,on/off}$ the buffet onset or offset model as as defined in Eq. (5) and Eq. (7), respectively.

The state dependent effects captured by $B_i(x)$ in Eq. (8) depend on the angle of attack, control surface deflections and dynamic pressure [29] and aeroelastic characteristics [28]). In this research, $B_i(x)$ is defined as a multivariate polynomial, the parameters of which are estimated using ordinary least squares parameter estimation. In this case, the state x was define to contain h (altitude), q, q/W (as the buffet intensity and frequency scale with q, whereas W accounts for the aeroelastic characteristics [28]), α and dV/dt (an increase in the deceleration rate, causes a more abrupt stall, which increases the duration of the stall and the intensity based on the flight test data). Each input is determined at the angle of attack where the lift coefficient is maximum as this was found to be the buffet onset point.

To simplify implementation, it is assumed that $B_i(x)$ are bivariate polynomials of degree $0 \leq d \leq 5$. The domain of these polynomials is determined by rectangular grids using the minimum and maximum values of the input data. A best fit for each of the four buffet models is achieved at the lowest Root Mean Squared Error (RMSE) value in combination with the largest Coefficient of Determination (R^2) value.

As buffet characteristics are encoded in $B_i(x)$ and $A_{i,on/off}$, tuning these parameters would yield a buffet model for other aircraft. In this research, data of the Cessna Citation is used to determine if a generalization of the buffet model is possible. The Cessna Citation II is a straight-wing, twinjet business jet aircraft, which characteristics differ substantially compared to the Fokker-100.

IV. Results

The buffet model was identified with a data set containing 92 recordings in the clean configuration and a data set containing 89 recordings in the landing configuration. A model training set and model validation set were chosen arbitrary, with a 60%-40 % split, in each configuration. In the first section, the results for the Fokker-100 buffet model are presented. Furthermore, the model quality of the buffet model is assessed and lastly, model validation is conducted using flight test data of the Cessna Citation II.

A. Fokker-100 Buffet Model

1. Flight-condition based buffet scaling

In the clean configuration, a total of 92 recordings are available, where a total of 54 recordings are used for training purposes and the remaining 38 are used for validation purposes, which roughly is a 60-40 split. Angle of attack and deceleration rate yielded the best results as inputs x for the flight-condition based buffet scaling $B_i(x)$ in clean configuration. In Figure 4 a slice through the flight envelope for the clean configuration are shown for both input terms, where the blue crosses indicate the points used for training and the black with red dots indicate the validation points. A flight envelope slice is given for the angles of attack and for the deceleration rate; in these slices the separation between test points is the largest. An underpopulated region in this flight envelope is at low angles of attack and high deceleration rates and at high angles of attack and low deceleration rates. It should be noted that in these underpopulated regions validation data is scarce, and hence the quality of the model cannot be guaranteed there.

For the buffet models in the landing configuration, a total of 88 recordings are available. From these 88 recordings, 52 are used for training and the remaining 36 are used for validation purposes, which is also roughly a 60-40 split. The most adequate fit was achieved using pressure altitude and dynamic pressure over weight as inputs x for $B_i(x)$, which can be seen in Figure 4. In this flight envelope slice, an underpopulated region can be found at low altitudes in combination with high values for dynamic pressure over weight, again limiting model validation in these regions.

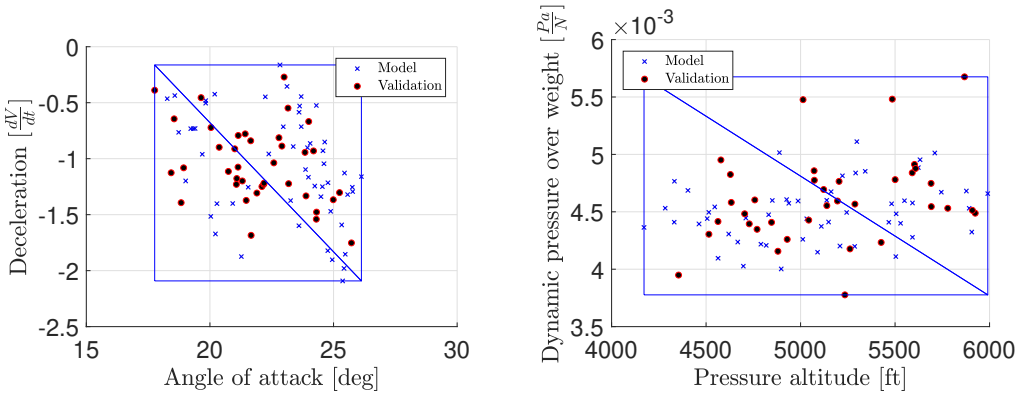

(a) Flight envelope slices in clean configuration in terms of angle of attack and deceleration rate.

(b) Flight envelope slice in landing configuration in terms of altitude and dynamic pressure over weight.

Fig. 4 Flight envelope slice in clean and landing configuration

2. On- and Offset Conditions

Buffet onset- and offset conditions were identified separately in both the vertical and lateral directions. However, buffet onset and offset yielded similar results as can be identified from Figure 5. Figure 5 only shows the buffet onset and offset in clean configuration, however, similar results were found for the landing configuration.

The buffet onset transient behavior, defined as the duration from buffet onset to maximum buffeting, was also calculated separately for all four buffet models. A median onset transient for accelerations in the lateral direction in the clean configuration is set at 0.70 s, whereas the median onset duration in the vertical direction in the clean configuration is 0.88 s. The median onset duration in landing configuration is set at 1.56 s in the lateral direction and 1.75 s in the vertical direction. The buffet onset duration in landing configuration in either direction is approximate twice the buffet onset duration in clean configuration.

Although similar recordings are used to calculate the buffet onset duration a difference in onset duration in the lateral and vertical direction is calculated. As normality of the onset transient time could not be assumed, a Wilcoxon signed-rank test is used to determine similarity in distributions for both populations. However, the null hypothesis was rejected, indicating that the onset time in the lateral direction and vertical direction do not come from a similar distribution. Therefore, the onset duration was set independently in each direction.

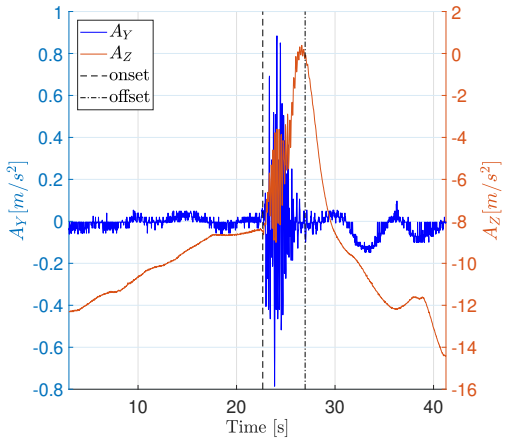

Fig. 5 Example measured accelerations in lateral and vertical direction including buffet onset and offset in clean configuration.

3. Frequency Response Fit

The frequency response fits in the lateral and vertical direction in the clean configuration are shown in Figure 6. The intensity of the vertical accelerations is approximately ten times larger than the intensity of the lateral accelerations, which indicates that accelerations in the vertical direction are most dominant in a stall. In the lateral direction, the four identified peak frequencies are located at 2.60 Hz, 4.40 Hz, 5.65 Hz and 7.62 Hz, whereas the three peak frequencies in the vertical direction are located at 4.80 Hz, 8.46 Hz and 13.37 Hz. In Table 2 the results for each parameter can be found. The Root Mean Square Error (RMSE) for the model in lateral direction is $5.9670{\cdot}10^{-5}\ \frac{m^2/s^4}{Hz}$, the relative Root Mean Square Error (RMS_{rel}) is 38.24%, whereas the coefficient of determination (R^2) equals 0.8162. The RMS in vertical direction is $1.6719{\cdot}10^{-4}\ \frac{m^2/s^4}{Hz}$, the RMS_{rel} is 13.61%, whereas the R^2 equals 0.9800. The low Cramer-Rao lower bounds from Table 2 in combination with the low RMSE values and high value for the R^2 indicates an adequate fit for the frequency response fit in both directions.

Figure 7 shows the frequency response fit for the accelerations in the lateral and vertical direction in the landing direction. In the landing configuration, the intensity in the vertical direction is also approximately ten times larger when compared to the intensity in the lateral direction, thus the stall buffet is also most dominant in the vertical direction. A total of four peak frequencies in the lateral direction are located at 2.60 Hz, 4.26 Hz, 5.89 Hz and 7.62 Hz, thus setting N in Eq. (3) to four. In the vertical direction, N is set to three as there are three peak frequencies at 4.89 Hz, 8.53 Hz and 13.51 Hz. All results of the iterative, nonlinear least squares method for both frequency responses can be found in Table 3. The RMSE for the frequency response fit in lateral direction in landing configuration is $1.4486{\cdot}10^{\mathbf{-4}}\ \frac{m^2/s^4}{Hz}$, the RMSE_{rel} is 38.14%, whereas the R^2 equals 0.8296 The RMSE for the fit in vertical direction in landing configuration

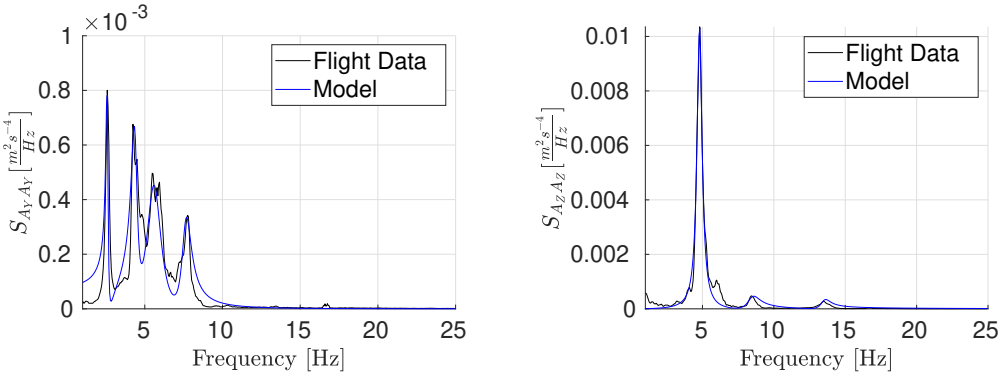

(a) Frequency response fit over 54 recordings for the lateral IRS acceleration measurements in the clean configuration.

(b) Frequency response fit over 54 recordings for the vertical IRS acceleration measurements in the clean configuration.

Fig. 6 Frequency response fit over 54 recordings for the lateral and vertical IRS acceleration measurements in the clean configuration.

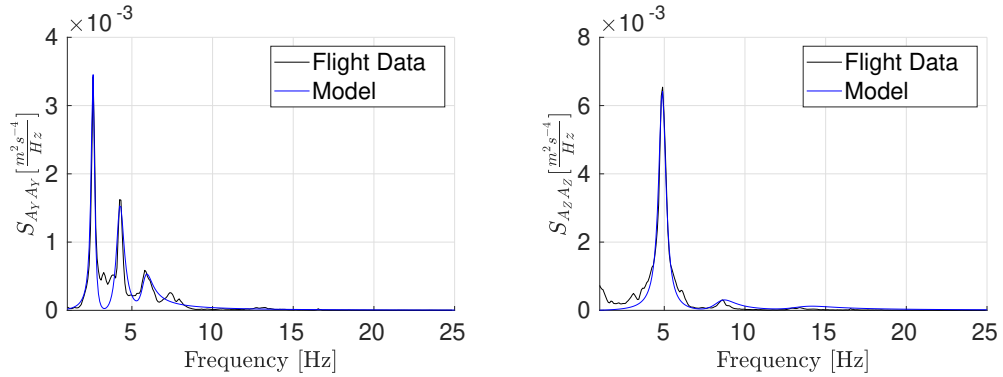

(a) Frequency response fit over 52 recordings for the lateral IRS acceleration measurements in the landing configuration.

(b) Frequency response fit over 52 recordings for the vertical IRS acceleration measurements in the landing configuration.

Fig. 7 Frequency response fit over 52 recordings for the lateral and vertical IRS acceleration measurements in the landing configuration.

is $1.5544 \cdot 10^{-4}$ $\frac{m^2/s^4}{Hz}$, the RMSE_{rel} is 17.77%, whereas the R^2 equals 0.9645. Also in the landing configuration, the low Cramer-Rao lower bounds and RMSE values in combination with a high value for the R^2 indicates an adequate frequency response fit for both directions.

4. Scaling polynomial parameter estimation

Figure 4 shows the flight envelope slices in which the flight test data was most clearly separated, yielding the best results for the scaling polynomial $B_i(x)$ in Eq. (8). In the clean configuration, the flight envelope is given by the angle of attack and the deceleration rate whereas for the landing configuration the flight envelope is given by the pressure altitude and dynamic pressure over weight. A second-order (quadratic) polynomial for all four models yielded the best results. An overview of the goodness-of-fit parameters is shown in Table 4.

The goodness-of-fit parameters RMSE_{rel} and R^2 in either configuration yield similar results, which indicates a similar gain proportion in either direction, due to buffet intensity per recording. Although the RMSE and relative RMSE show low values, the R^2 value is also rather low, which indicates that the model output does not entirely represent the buffet intensity. A low value for the R^2 is due to the scarceness of the data points in some regions of the flight envelope.

Lastly, one time series for the measured accelerations including the buffet models for each combination of configuration and direction are shown in Figure 8 and Figure 9. In each subfigure, the blue lines indicate the measured flight test data, whereas the red lines are the model output based on Eq. (8). The subfigures in the left column show an entire flight recording, whereas the recordings on the right zoom in on the buffet part of the flight recording.

Table 2 Parameter estimates for the frequency response function in the lateral and vertical direction in the clean configuration.

		Lateral direction			Vertical direction		
		$\hat{\zeta}$	$\sigma(\hat{\zeta})$	$\frac{\sigma(\hat{\zeta})]}{\hat{\zeta}} \cdot 100$	$\hat{\zeta}$	$\sigma(\hat{\zeta})$	$\frac{\sigma(\hat{\zeta})]}{\hat{\zeta}} \cdot 100$
K_1	[-]	0.00159	$1.5080 \cdot 10^{-4}$	9.4974	0.10141	$8.5484 \cdot 10^{-4}$	0.8430
ω_1	[rad/s]	16.3326	$7.4838 \cdot 10^{-3}$	0.0458	30.1651	$1.7625 \cdot 10^{-2}$	0.0584
Q_1	[-]	15.0121	$1.4137 \cdot 10^{-3}$	0.0094	11.1269	$1.7369 \cdot 10^{-3}$	0.0156
K_2	[-]	0.00201	$3.7879 \cdot 10^{-4}$	18.814	0.01923	$7.1283 \cdot 10^{-4}$	3.7077
ω_2	[rad/s]	27.6503	$7.0717 \cdot 10^{-2}$	0.2558	53.1809	$2.5656 \cdot 10^{-1}$	0.4824
Q_2	[-]	9.17651	$7.8483 \cdot 10^{-3}$	0.0855	7.82235	$1.3992 \cdot 10^{-2}$	0.1789
K_3	[-]	0.00417	$2.3332 \cdot 10^{-4}$	5.5888	0.01320	$3.7902 \cdot 10^{-4}$	2.8709
ω_3	[rad/s]	35.4808	$9.6524 \cdot 10^{-2}$	0.2720	83.9878	$4.0341 \cdot 10^{-1}$	0.4803
Q_3	[-]	4.78712	$9.4047 \cdot 10^{-3}$	0.1965	13.5702	$9.4468 \cdot 10^{-3}$	0.0696
K_4	[-]	0.00151	$1.5996 \cdot 10^{-4}$	10.572			
ω_4	[rad/s]	47.9013	$6.4145 \cdot 10^{-2}$	0.1339			
Q_4	[-]	4.78712	$4.0835 \cdot 10^{-3}$	0.0401			

Table 3 Parameter estimates for the frequency response function in the lateral and vertical direction in the landing configuration.

		Lateral direction			Vertical direction		
		$\hat{\zeta}$	$\sigma(\hat{\zeta})$	$\frac{\sigma(\hat{\zeta})}{\hat{\zeta}} \cdot 100$	$\hat{\zeta}$	$\sigma(\hat{\zeta})$	$\frac{\sigma(\hat{\zeta})}{\hat{\zeta}} \cdot 100$
H_1	[-]	0.05758	$3.1835 \cdot 10^{-4}$	0.5564	0.07970	$1.3432 \cdot 10^{-3}$	1.6823
ω_1	[rad/s]	16.3337	$9.2457 \cdot 10^{-3}$	0.0568	30.7010	$5.7144 \cdot 10^{-2}$	0.1860
Q_1	[-]	10.1452	$1.5864 \cdot 10^{-3}$	0.0157	8.88653	$4.5758 \cdot 10^{-3}$	0.0515
H_2	[-]	0.03799	$1.6819 \cdot 10^{-3}$	4.5236	0.01478	$4.7843 \cdot 10^{-4}$	3.2280
ω_2	[rad/s]	26.7751	$1.7212 \cdot 10^{-1}$	0.6438	53.6058	$3.6428 \cdot 10^{-1}$	0.6835
Q_2	[-]	7.18551	$1.9449 \cdot 10^{-2}$	0.2723	5.14542	$2.2158 \cdot 10^{-2}$	0.4340
H_3	[-]	0.01696	$4.4032 \cdot 10^{-4}$	1.9170	0.00736	$1.5068 \cdot 10^{-4}$	2.0323
ω_3	[rad/s]	37.0136	$1.4573 \cdot 10^{-1}$	0.3943	84.7993	$4.6090 \cdot 10^{-1}$	0.5439
Q_3	[-]	7.32298	$1.1963 \cdot 10^{-2}$	0.2245	4.29687	$1.8046 \cdot 10^{-2}$	0.4207
H_4	[-]	0.00120	$1.6003 \cdot 10^{-4}$	13.278			
ω_4	[rad/s]	47.9320	$6.4154 \cdot 10^{-2}$	0.1339			
Q_4	[-]	0.13121	$4.1020 \cdot 10^{-3}$	3.1121			

Table 4 Goodness-of-fit for the second-order polynomial in the clean and landing configuration.

(a) Goodness-of-fit for the second-order polynomial in the landing configuration.

		Lateral direction	Vertical direction
RMSE	[-]	1.709	2.051
RMSE_{rel}	[%]	15.55	14.98
R^2	[-]	0.621	0.642

(b) Goodness-of-fit for the second-order polynomial in the clean configuration.

		Lateral direction	Vertical direction
RMSE	[-]	2.158	3.476
RMSE_{rel}	[%]	24.06	24.05
R^2	[-]	0.572	0.572

B. Fokker-100 Buffet Model Analysis and Quality Assessment

In this section, a more in-depth analysis of the results is conducted. Additionally, the Fokker-100 model quality is assessed in terms of the goodness-of-fit parameters RMS, RMS_{rel} and R^2.

First of all, the buffet onset transient duration in each buffet model was tested for normality using the Shapiro–Wilk test and the one-sample Kolmogorov-Smirnov test. However, low p-values indicated that the hypothesis was rejected, such that normality could not be assumed. Therefore, a median onset duration is defined in each of the four models. Although, similar recordings are used to determine the onset duration a difference in onset duration was calculated. Therefore, a Wilcoxon signed ranked test determined if the onset duration still came from a similar distribution. However, the hypothesis of the Wilcoxon signed-rank test was rejected, indicating that the onset duration in lateral and vertical direction does not come from similar distribution. The definition of the maximum buffet intensity could indicate why the onset duration is lower for the accelerations in the lateral direction. In the lateral direction the standard deviations are $\sigma = 0.0847$ m/s^2 and $\sigma = 0.0732$ m/s^2, whereas in the vertical direction the standard deviation are $\sigma = 0.1045$ m/s^2 and $\sigma = 0.1171$ m/s^2 in the clean and landing configurations, respectively. Lower values in the lateral direction

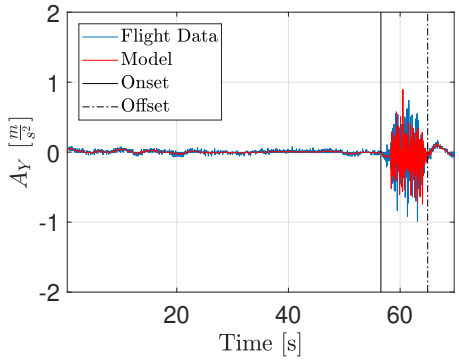

(a) Measured lateral acceleration including the lateral buffet model in the clean configuration.

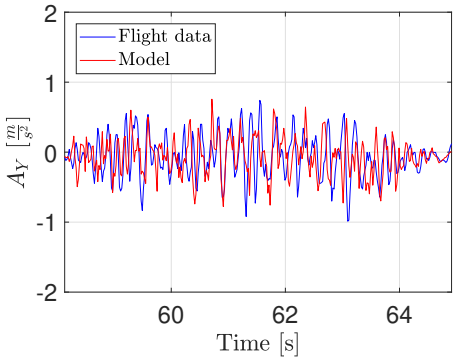

(b) Measured lateral acceleration including the lateral buffet model in the clean configuration (zoomed in on the buffet).

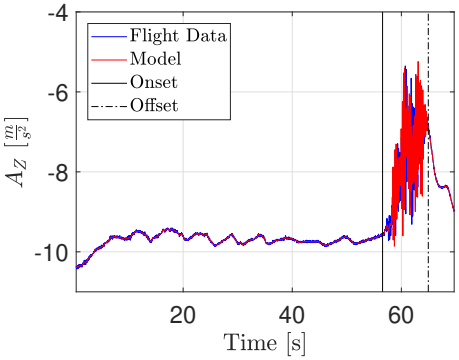

(c) Measured vertical acceleration including the vertical buffet model in the clean configuration.

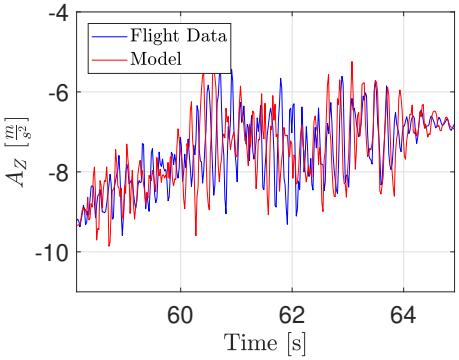

(d) Measured vertical acceleration including the vertical buffet model in the clean configuration (zoomed in on the buffet).

Fig. 8 Measured accelerations and buffet models in the lateral and vertical direction for the clean configuration.

could indicate that the buffet onset duration is reached earlier. A difference in onset duration is also possible due to the separation of the flow. Flow separation for wings-level stall maneuvers usually gradually separates from the wing, inducing a turbulent airflow that may already have a stronger effect on the vertical stabilizer. Additionally, the median buffet onset time for the model in landing configuration is approximately twice as long as the buffet onset time in clean configuration. A stall in clean configuration requires thus less time to reach maximum buffet intensity when compared to a stall in the landing configuration.

Secondly, in the vertical direction in clean and landing configuration a total of three peak frequencies were identified whereas in the lateral direction four peak frequencies were identified, as can be seen in Table 3 and Table 5. An overview of all frequencies is given in Table 6. The peak frequency values are similar in their respective direction, independent of the aircraft configuration. These similarities correspond to the type-specific eigenmode shapes of the Fokker-100 aircraft. The three peak frequencies in the vertical direction are approximately located at 4.85 Hz, 8.50 Hz and 13.5 Hz and correspond to the fuselage vertical bending, second-order wing bending, and vertical stabilizer bending, respectively. In the lateral direction, these frequencies are located at 2.60 Hz, 4.30 Hz, 5.75 Hz and 7.62 Hz, which are the asymmetrical fin bending, asymmetrical fin torsion, fuselage lateral bending and the lateral wing bending modes.

An overview of the goodness-of-fit parameters for the buffet model in the vertical direction and lateral direction is given in Table 6 and Table 7 respectively. In each of the four buffet models, a higher R^2 value and lower RMSE and RMSE_{rel} values indicate a better fit for the frequency response compared to the polynomial fit. An increase in buffet model accuracy is likely to be achieved by increasing the accuracy of the buffet transient. The goodness-of-fit parameters indicate a better fit for the buffet models in the vertical direction in their respective configuration when compared to the buffet models in the lateral direction. A more accurate fit in the vertical direction is required as the accelerations in

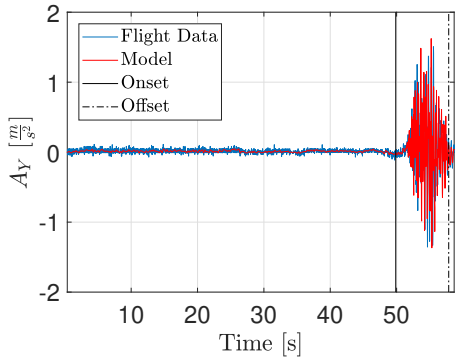

(a) Measured lateral accelerations including the lateral buffet model in the landing configuration.

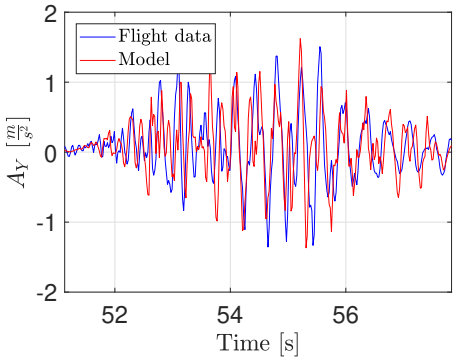

(b) Measured lateral acceleration including the lateral buffet model in the landing configuration (zoomed in on the buffet).

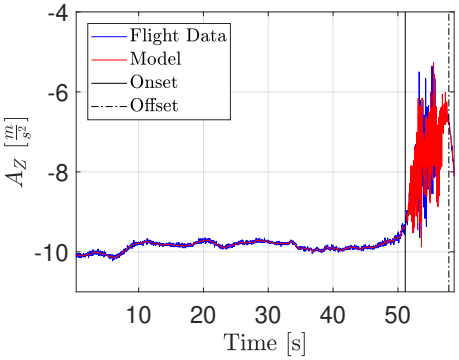

(c) Measured vertical accelerations including the vertical buffet model in the landing configuration.

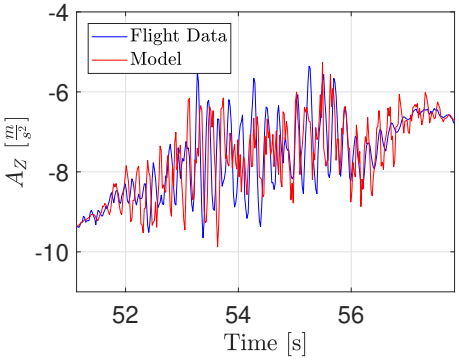

(d) Measured vertical acceleration including the vertical buffet model in the landing configuration (zoomed in on the buffet).

Fig. 9 Measured accelerations and buffet models in the lateral and vertical direction for the landing configuration.

Table 5 Frequency mode-shapes for the Fokker-100.

		Clean configuration		Landing configuration	
		Lateral direction	Vertical direction	Lateral direction	Vertical direction
f_1	[Hz]	2.60	4.80	2.60	4.89
f_2	[Hz]	4.40	8.46	4.26	8.53
f_3	[Hz]	5.65	13.37	5.89	13.51
f_4	[Hz]	7.62	-	7.62	-

vertical direction were identified as most dominant in a stall. The buffet models in the landing configuration have a better fit compared to the buffet models in the clean configuration.

Table 6 Goodness-of-fit parameters for the buffet models in vertical direction.

	Clean configuration				Landing configuration			
	Frequency response fit		Polynomial fit		Frequency response fit		Polynomial fit	
RMSE	$1.6719 \cdot 10^{-4}$	$\frac{m^2/s^4}{Hz}$	3.476	-	$1.5544 \cdot 10^{-4}$	$\frac{m^2/s^4}{Hz}$	2.051	-
RMSE_{rel}	13.61	%	24.05	%	17.77	%	14.98	%
R^2	0.9800	-	0.572	-	0.9645	-	0.642	-

The total buffet model is modeled according to Eq. (8), which is a white noise signal passed through a shaping filter, multiplied with a gain and added to the baseline acceleration. Although Figure 8 and Figure 9 show adequate buffet behavior, including buffet onset and offset, a combination of parameters influence the model validity and model quality.

Table 7 Goodness-of-fit parameters for the buffet models in lateral direction.

	Clean configuration				Landing configuration			
	Frequency response fit		Polynomial fit		Frequency response fit		Polynomial fit	
RMSE	$5.9670 \cdot 10^{-5}$	$\frac{m^2/s^4}{Hz}$	2.158	-	$1.4486 \cdot 10^{-4}$	$\frac{m^2/s^4}{Hz}$	1.709	-
$RMSE_{rel}$	38.42	%	24.06	%	38.41	%	15.55	%
R^2	0.8162	-	0.572	-	0.8296	-	0.621	-

First of all, the validity of each of the buffet models is given in Figure 4 in combination with the flight envelope of Figure 4. Any likely combination of input parameter for each buffet model within the valid flight envelope resulted in a positive value for the gain, indicating the gain scheduling procedure is modeled adequately. Secondly, a difference in model output and measured value might be due to the random nature of the colored noise in combination with the estimated gain and acceleration as well as the non-linearity in a stall buffet. Even so, the low RMSE values indicate that the output of the buffet model might still be within the 95% interval. Lastly, a median onset duration was used in each model, therefore the maximum buffet intensity might be reached later than the median value.

C. Model Quality Assessment using Cessna Citation II Flight Test Data

In addition to the model quality analysis of the Fokker-100 stall buffet model, another validation set is applied using the Fokker-100 stall buffet methodology. The validation set is based on the flight test data of the Cessna Citation II as described in [25]. The data set contains a total of 69 quasi-steady stall maneuvers in clean configuration, where 54 flight recordings are used for model training and 15 flight recordings for model validation. Validation is only conducted in the clean configuration for the accelerations in the vertical direction.

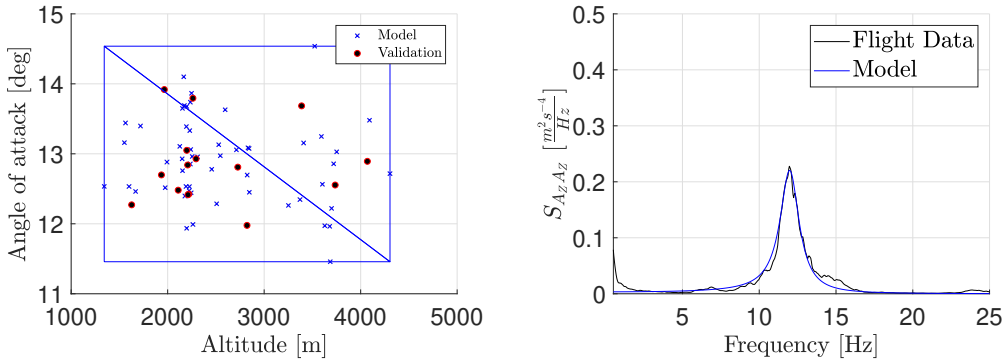

(a) Flight envelope in terms of angle of attack and altitude in the clean configuration.

(b) Frequency response fit over 54 recordings for the vertical IRS acceleration measurements in the clean configuration.

Fig. 10 Frequency response fit and flight envelope in the vertical direction in the clean configuration for the Cessna Citation II.

For the Cessna Citation, the flight envelope slice in the clean configuration in terms of angle of attack and altitude, shown in Figure 10, yielded the best goodness-of-fit parameters for the scaling polynomial $B_i(x)$. The validity of the Cessna Citation flight envelope is at lower angles of attack and altitudes when compared to the flight envelope of the Fokker-100. The median buffet onset duration for the Cessna Citation stall maneuvers is 0.45 seconds. Buffet offset occurs at a change in the change in the sign of $\dot{\alpha}$ in combination with exceeding the angle of attack threshold of 10 degrees. However, due to the dynamic stability of the Cessna Citation, an additional constraint for the buffet offset is required. In several stall maneuvers, two or more consecutive stalls were flown, as indicated by the increasing angle of attack after the initial stall in Figure 11. In Figure 11, buffet onset and offset occurs twice for the Cessna Citation, but only once for the Fokker-100. Therefore, in addition to the current buffet offset conditions, the buffet offset was set to a different value for $\dot{\alpha}$ as long as the angle of attack is above ten degrees. In Figure 10 the frequency response fit for the vertical direction is also shown. The peak-frequency in the vertical direction is located at 12 Hertz, whereas the highest peak-frequency for the Fokker-100 is located at 4.80 Hertz, indicating a difference in structural eigenmode-shapes.

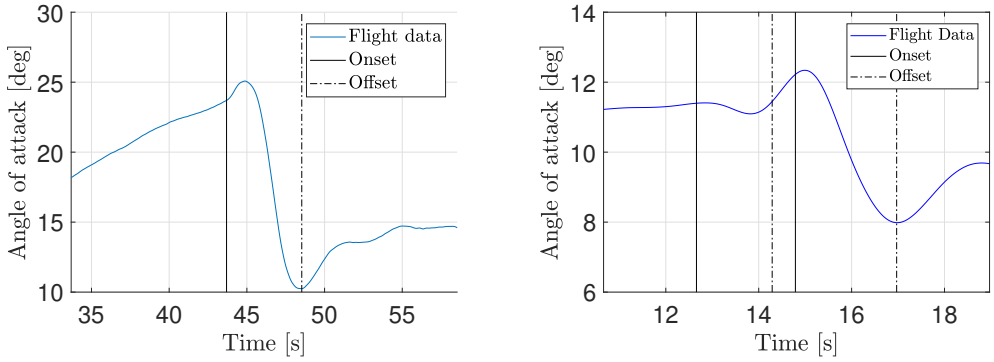

(a) Angle of attack including buffet onset and offset for the Fokker-100.

(b) Angle of attack including buffet onset and offset for the Cessna Citation II.

Fig. 11 Angle of attack including buffet onset and offset for the Fokker-100 and Cessna Citation in clean configuration.

In Table 8 the goodness-of-fit for the buffet model in the vertical direction and clean configuration the Fokker-100 and Cessna Citation is shown. The frequency response fit for the Cessna Citation is adapted from [25].

Table 8 Goodness-of-fit parameters in the vertical direction in the clean configuration for the Fokker-100 and Cessna Citation II.

(a) Goodness-of-fit parameters in the vertical direction in the clean configuration for the Fokker-100.

	Frequency response fit		Polynomial fit	
RMSE	$1.6719 \cdot 10^{-4}$	$\frac{m^2/s^4}{Hz}$	3.476	-
RMSE_{rel}	13.61	%	24.05	%
R^2	0.9800	-	0.572	-

(b) Goodness-of-fit parameters in the vertical direction in the clean configuration for the Cessna Citation II.

	Frequency response fit		Polynomial fit	
RMSE	$1.1189 \cdot 10^{-4}$	$\frac{m^2/s^4}{Hz}$	0.2732	-
RMSE_{rel}	-	%	11.15	%
R^2	0.9731	-	0.6234	-

In Figure 12 the measured accelerations and buffet model in the vertical direction for the Cessna Citation are shown. In the figures the onset and offset conditions are indicated by the solid and dashed black lines. Figure 12(b) and (c) show zoomed-in views of the buffet model's output, where the window is defined from buffet onset to buffet offset.

A similar frequency response fit in terms of R^2 and RMSE indicate that the Fokker-100 stall buffet model methodology can be adapted to the Cessna Citation II with relatively minor modifications, hence proving generalization to different aircraft types. However, the generalization of the methodology requires type-specific parameters to be available or determined from the flight test data. First of all, the flight envelopes for both aircraft differ, which requires specific knowledge on some stall related parameters, for example, the critical angle of attack. Secondly, the buffet frequency response fit for either aircraft has to be calculated from the accelerations in the flight test data. A combination of the frequency response fit and the flight envelope also determine the values of the scheduled gains. Thirdly, the buffet onset duration has to be estimated for the different aircraft types in each direction. Lastly, the similarity in maneuvers in the flight test data should be flown. However, by setting an additional buffet offset constraint the similarity in-flight maneuver might be mitigated to some extent. However, if each of these type-specific aircraft parameters is determined, the stall buffet methodology in this research is a step towards a more generic buffet model.

V. Conclusion

In this paper, a methodology is presented to model the stall buffet component using flight test data from the swept-wing Fokker-100 medium-sized transport aircraft. The stall maneuvers were flown according to JAR-25 flight certification tests. A total of four separate models were identified, one model for each combination of the clean and landing configuration and the lateral and vertical accelerations. Validation indicated adequate goodness-of-fit parameters for each of the four buffet models. An additional validation in the clean configuration in the vertical direction using straight wing flight test data was conducted. The methodology showed to be generalizable when type-specific aircraft

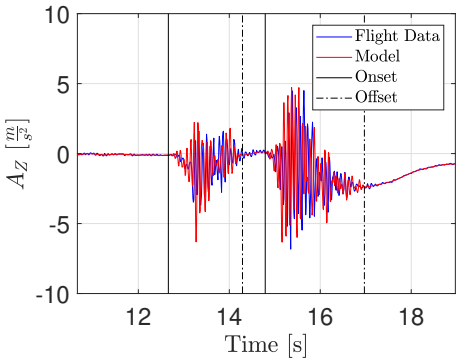

(a) Measured vertical acceleration including the vertical buffet model in clean configuration.

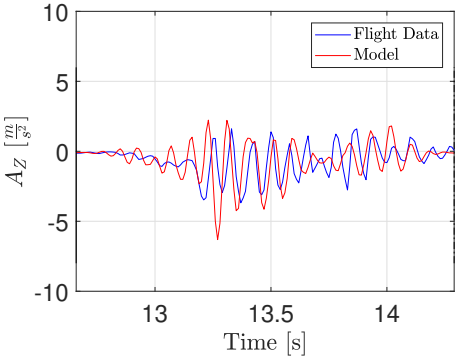

(b) Measured vertical acceleration including the vertical buffet model in the clean configuration (zoomed in on the first buffet).

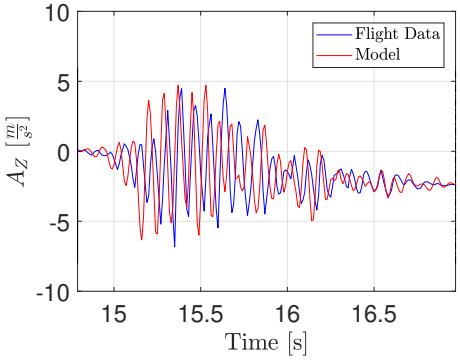

(c) Measured vertical acceleration including the vertical buffet model in the clean configuration (zoomed in on the second buffet).

Fig. 12 Measured accelerations and buffet model in the vertical direction and the clean configuration for the Cessna Citation II.

characteristics are available. The stall buffet model output adequately represents the highly nonlinear buffeting in the flight test data.

In this research, the buffet onset is triggered after two conditions are met, that is, the critical angle of attack is exceeded (17.5 degrees for the Fokker-100), and a (sustained) change in the sign of the slope of the $C_L - \alpha$ curve from positive to negative. A transient onset behavior is modeled using the median time duration for the buffet to reach the maximum buffet intensity. The maximum buffet intensity is defined as the accelerations within the 95% confidence interval. The buffet onset duration was assumed to be scaled quadratically up to the maximum buffet intensity. The buffet offset point, the point where buffet effects receded, occurred at angles of attack lower than 15.0 degrees when the angle of attack started increasing again. The flight test data showed that buffet offset occurs at exceeding a zero angle of attack rate.

The buffet transient is identified by shaping a white noise signal and multiplying the signal with a gain. A combination of N second-order band-pass filters is used as shaping filters, where N is the number of identified peak frequencies from a periodogram, which represents Fokker-100 specific eigenmode-shapes. A bivariate second-order polynomial models the buffet intensity as a function of the aircraft states. Adequate goodness-of-fit parameters for the frequency response fit and polynomial fit were obtained in each model.

Additional validation was conducted using straight wing flight test data from the Cessna Citation. When type-specific parameters are available, the buffet model methodology also applies to other aircraft types. In conclusion, a more generic methodology for identifying a buffet model for different aircraft is identified. The buffet model methodology could positively contribute to increased pilot awareness in flight simulation training devices as buffeting is a key characteristic of the stall. Ultimately, combining this research with concurrent research could mitigate LOC-I occurrences.

References

[1] Lemley, C. and Mullans, R., *Buffeting pressures on a swept wing in transonic flight - Comparison of model and full scale measurements*, Structures, Structural Dynamics, and Materials and Co-located Conferences, chapter and pages. Doi:10.2514/6.1973-311.

[2] Caruana, D., Correge, M., Reberga, O., Despre, C. & Mignosi, A., *Buffet and buffeting active control*, Fluid Dynamics and Co-located Conferences, chapter and pages. Doi:10.2514/6.2000-2609.

[3] Dang, H., and Yang, Z. , "Buffet Onset Prediction and Flow Field Around a Buffeting Airfoil at Transonic Speeds," *In 51st AIAA/ASME/ASCE/AHS/ASC Structures, Structural Dynamics, and Materials Conference: American Institute of Aeronautics and Astronautics.*, 2010. Doi:10.2514/6.2010-3051.

[4] Liguore, S. and Pitt, D., "Aircraft Buffet Prediction Using Unsteady Aerodynamic Wind Tunnel Model Six-Component Balance Data." *In 45th AIAA/ASME/ASCE/AHS/ASC Structures, Structural Dynamics & Materials Conference: American Institute of Aeronautics and Astronautics.*, 2004. Doi:10.2514/6.2004-2045.

[5] Bérard, A., Rizz, A. & Isikveren, A.T., "Development and Implementation of Aerodynamic Analysis Methods for Aircraft Conceptual Design ," *Canadian Aeronautics and Space Institute Annual General Meeting. Aircraft Design & Development Symposium.*, 2007. Retrieved on March 13, 2019, from https://www.researchgate.net/publication/274706692_Development_and_Implementation_of_Aerodynamic_Analysis_Methods_for_Aircraft_Conceptual_Design.

[6] Huston, W.B., Rainey, A.G. & Baker, T.F., "*A Study of the Correlation Between Flight and Wind-Tunnel Buffeting Loads*," (Technical Report NACA-RM-L55E16b)., Langley Field, VA, United States: National Advisory Committee for Aeronautics. Langley Aeronautical Lab., 1955.

[7] Skopinski, T.H. and Huston, W.B., "*A semi-empirical procedure for estimating wing buffet loads in the transonic region*," (Technical Report NACA-RM-L56E01)., Langley Field, VA, United States: National Advisory Committee for Aeronautics. Langley Aeronautical Lab., 1956.

[8] Davis, D.D., Jr and Wornom, D.E., "*Buffet Tests of an Attack-airplane Model with Emphasis on Analysis of Data from Wind-tunnel Tests*," (Technical Report NACA-RM-L57H13)., Langley Field, VA, United States: National Advisory Committee for Aeronautics. Langley Aeronautical Lab., 1957.

[9] Brunet, V., *Computational Study of Buffet Phenomenon with Unsteady RANS Equations*, Fluid Dynamics and Co-located Conferences, chapter and pages. Doi:10.2514/6.2003-3679.

[10] Lawson, S., Greenwell, D & Quinn, M.K., *Characterisation of Buffet on a Civil Aircraft Wing*, AIAA SciTech Forum, chapter and pages. Doi:10.2514/6.2016-1309.

[11] van Eijndhoven, J.N.A., "Buffet envelope prediction of transport aircraft during the conceptual design phase: Predict transonic, shock induced buffet onset," Master's thesis, Delft University of Technology, 2012.

[12] Mabey, D., "Some aspects of aircraft dynamic loads due to flow separation," *Progress in Aerospace Sciences*, Vol. 26, No. 2, 1989, pp. 115–151. Https://doi.org/10.1016/0376-0421(89)90006-7.

[13] Mabey, D., "Review of the normal force fluctuations on aerofoils with separated flow," *Progress in Aerospace Sciences*, Vol. 29, No. 1, 1992, pp. 43–80. Https://doi.org/10.1016/0376-0421(92)90003-Z.

[14] Bérard, A. and Isikveren, A.T., "Conceptual Design Prediction of the Buffet Envelope of Transport Aircraft," *Journal of Aircraft*, Vol. 46, No. 5, 2009, pp. 1593–1606. Doi: 10.2514/1.41367.

[15] Boeing, "Statistical Summary of Commercial Jet Airplane Accidents," , 2016. Retrieved on September 27, 2018, from http://www.boeing.com/resources/boeingdotcom/company/about_bca/pdf/statsum.pdf.

[16] Airbus S.A.S., "A Statistical Analysis of Commercial Aviation Accidents 1958-2017," , 2017. Retrieved on September 27, 2018, from https://www.airbus.com/content/dam/corporate-topics/publications/safety-first/Airbus-Commercial-Aviation-Accidents-1958-2017.pdf.

[17] International Civil Aviation Organization, "2018 Safety Report," , 2018. Retrieved on September 27, 2018, from https://www.icao.int/safety/Documents/ICAO_SR_2018_30082018.pdf.

[18] International Air Transport Association, "Loss of Control In-Flight Accident Analysis Report," , 2015. Retrieved on September 27, 2018, from https://www.iata.org/whatwedo/safety/Documents/LOC-I-1st-Ed-2015.pdf.

[19] Jacboson, S.R., "*Aircraft Loss of Control Causal Factors and Mitigation Challenges*," (Technical Report DFRC-E-DAA-TN1949)., Edwards, CA, United States: NASA Dryden Flight Research Center, 2010.

[20] Crider, D.A., *Need for Upset Recovery Training*, Guidance, Navigation, and Control and Co-located Conferences, chapter and pages. Doi:10.2514/6.2008-6864.

[21] European Aviation Safety Agency, "Opinion No 06/2017," , 2017. Retrieved on October 2, 2018, from https://www.easa.europa.eu/sites/default/files/dfu/Opinion%20No%2006-2017.pdf .

[22] Federal Aviation Administration, "120-109A - Stall Prevention and Recovery Training with Change 1," , 2017. Retrieved on October 2, 2018, from https://www.faa.gov/documentLibrary/media/Advisory_Circular/AC_120-109A_CHG_1.pdf .

[23] Federal Aviation Administration, "AC 120-111 - Upset Prevention and Recovery Training - with Change," , 2017. Retrieved on October 2, 2018, from https://www.faa.gov/documentLibrary/media/Advisory_Circular/AC_120-111_CHG_1.pdf .

[24] Abramov, N.B., Goman, M.G., Khrabrov, A.N., Kolesnikov, E.N., and Fucke, L., Soemarwoto, B. & Smaili, H., *Pushing Ahead - SUPRA Airplane Model for Upset Recovery*, Guidance, Navigation, and Control and Co-located Conferences, chapter and pages.

[25] van Horssen, L.J., de Visser, C.C. & Pool, D.M., "Aerodynamic Stall and Buffet Modeling for the Cessna Citation II Based on Flight Test Data," *In 2018 AIAA Modeling and Simulation Technologies Conference: American Institute of Aeronautics and Astronautics.*, 2018. Doi: 10.2514/6.2018-1167.

[26] Advani, S. and Field, J., "Upset Prevention and Recovery Training in Flight Simulators," *In AIAA Modeling and Simulation Technologies Conference: American Institute of Aeronautics and Astronautics*, 2011. Doi:10.2514/6.2011-6698.

[27] Schroeder, J.A., Burki-Cohen, J.S., Shikany, D., Gingras, D.R., & Desrochers, P.P. , "An Evaluation of Several Stall Models for Commercial Transport Training," *In AIAA Modeling and Simulation Technologies Conference: American Institute of Aeronautics and Astronautics.*, 2014. doi:10.2514/6.2014-1002.

[28] Courtland, D.P., *Stability and Control: Flight Testing*, 2nd ed., Pergamon, The Boulevard, Langford Lane, Kidlington ,Oxford, 2014.

[29] Danowsky, B.P. and Schulze, P.C., *Control Surface Buffet Load Measurement using Aircraft Actuators*, AIAA SciTech Forum, chapter and pages. Doi:10.2514/6.2016-2005.